The Microstructure and Mechanical Behavior of TRIP 800 and DP 1000 Steels Welded by Electron Beam Welding Method

Cihangir Tevfik Sezgin[1] , Fatih Hayat[2]

[1] Kastamonu University, Cide Rıfat Ilgaz Vocational School, Welding Technology, Cide, Kastamonu, Turkey.
[2] Karabük University, Faculty of Engineering, Metallurgy and Materials Engineering, Karabük, Turkey.

Abstract: TRIP 800 steel and DP 1000 steel welded by using the electron beam welding (EBW) method were investigated in this study. Martensite was a dominant phase at the fusion zone (FZ) of both steels. In addition, bainite and austenite were observed in the FZ of TRIP 800. The hardness of FZ and heat affected zone (HAZ) of both steels were higher than their base metals. The hardness of FZ of the TRIP 800 joinings was higher than the FZ of DP 1000. Ductility and tensile strength decreased at both of the joinings. However, this decrease became higher at the DP 1000 steel joinings compared to the TRIP 800 joinings. It was observed that the TRIP 800 joining absorbed more energy than the DP 1000 joining at impact notch test for each temperature.

Key-words: Transformation induced plasticity steel; Dual phase steel; Microstructure; Electron beam welding; Tensile strength.

1. Introduction

Automotive manufacturers need of developing new types of steel due to the energy crisis, increased in-car safety factors and environmental laws. Transformation induced plasticity (TRIP) and dual phase (DP) steels are considered as advanced high-strength steel (AHSS) [1]. Automotive manufacturers have extensively used both DP and TRIP steels to improve vehicle safety and reducing vehicle weight.

The TRIP steels have an unrivalled combination of excellent energy absorption, formability and strength properties [2]. These steels generally contain three phases, namely ferrite, retained austenite and bainite. However, the TRIP steels can also contain martensite [3]. The TRIP steels are extremely suitable for the automotive industry as a type of steel with high strength, excellent ductility and good vehicle collision resistance [4]. They are also highly favored for their perfect crash behaviour and high energy absorption at dynamic strain rates [5]. The TRIP steels with medium Mn content are suitable for automotive components where the full TRIP effect can be used [6].

The name DP steels refer to two dominant phases found in the microstructure: ferrite and martensite [7]. The DP steels contain a hard martensite phase, which is a secondary structure in a ferritic (soft) structure [8]. Due to the characteristic mechanical properties of their ferritic-martensitic microstructure, the DP steels have low yield strength, good ductility and high tensile strength. As the martensite ratio increases, the strength of the sheet increases while the formability property decreases [9].

Electron beam welding (EBW) is generally used in the defense and aerospace industries. EBW is one of the most advanced features of electron beam sources. With EBW, it is possible to weld without a filler metal in materials with thickness from 0.01 mm up to 250 mm for steel and up to 500 mm for aluminum and the vacuum environment has a minimum level of material oxygen related [10]. Welding dissimilar materials also becomes possible with EBW [11,12]. Furthermore, EBW is also used for welding refractory metals and chemically active metals which are otherwise hard to weld by other welding methods [10]. Despite all these advantages, its high investment cost has been limiting the usage areas of EBW.

There are studies in the literature reporting the weldability and post-weld strength values of DP steels and TRIP steels with welding methods such as gas metal arc welding (GMAW) [13,14], laser beam welding (LBW) [15,16] and resistance spot welding (RSW) [17,18]. There is some studies about advanced high strength steels are used at automotive industry welded by EBW [19-21]. However, no studies regarding the welding of DP or TRIP steels by using EBW were found in the literature. EBW has proven to be a highly credible welding method for joining new advanced steels such as TRIP/TWIP (TWinning Induced Plasticity) steel [22]. Therefore, it is important to examine how EBW affects the microstructure and mechanical properties of DP and TRIP steels. Because the one of the narrowest HAZ gets with EBW within all kinds of welding methods. So this is very important for aircraft and defence industries. High strength steel structures like TRIP and DP can be used to replace mild steel grades, allowing for the structure to be

made lighter. This can potentially increase the payload of vehicles and equipment are used for military and aircraft and reduce the fuel consumption whilst still retaining the structural integrity of the product. Kasonde observed ballistic performance of TRIP steel. His results even showed a relationship between the amount of transformation (in the impact zone) and the steel's ballistic performance [23]. Furthermore DP and TRIP steels have high impact strength and they can be used for perforated steel armour. Because perforated plates are also attractive for passive mitigation systems against explosive blast [24].

In this study, it was aimed to investigate the metallurgical structure of the weld zone (FZ), strength values such as hardness, tensile strength, toughness and elongation percentages of the welded parts by similar combining TRIP 800 and DP 1000 steels with the EBW welding method.

2. Experimental Details

In this study, TRIP 800 and DP 1000, which are new generation high strength steels, were used. The thickness of the TRIP 800 steel was 1.5 mm while the thickness of the DP 1000 steel was 1.2 mm. The chemical analysis of the sheets of both steels is shown in Table 1. The chemical composition of steels were given by import firms.In Table 2, the yield strength and the elongation and tensile strength of the base metal are shown. These results measured by us. At the beginning, EBW experiments were carried out to use varying beam current and welding speed. Such an exercise was necessary to understand their effects on weld bead profile and to optimize the process parameters in achieving full penetration. Although there was no penetration at 15 and 20 mA full penetration was ensured at 25 mA. Welding speeds were 150, 200 and 250 mm/minute, respectively. It was observed that 250 mm/minute was the optimum welding speed. The parameters of the welding machine are shown in Table 3.

Table 1. The chemical composition of the steels in wt.%.

Steel	C	Si	Mn	Al	Mo	Ni	Nb	V	P	S
TRIP 800	0.18	1.72	1.69	0.03	0.03	0.07	0.05	0.01	0.01	0.007
DP 1000	0.15	0.51	1.49	0.05	0.01	0.03	0.02	0.01	0.01	0.002

Table 2. Mechanical properties of the steels.

Steel	Yield Strength (MPa)	Tensile Strength (MPa)	Elongation (%)
TRIP 800	525	883	36
DP 1000	787	1091	8

Table 3. Welding parameters.

Welding Parameters	Value
Voltage (KV)	40
Ampere (mA)	25
The speed of mirror (mm/minute)	200
Pressure (Torr)	10^{-4}

The welded samples of TRIP 800 are shown in Figure 1. Figure 2 shows the samples which were used in the tensile strength, impact notch strength and microhardness tests. Figure 3 shows welded samples of DP 1000.
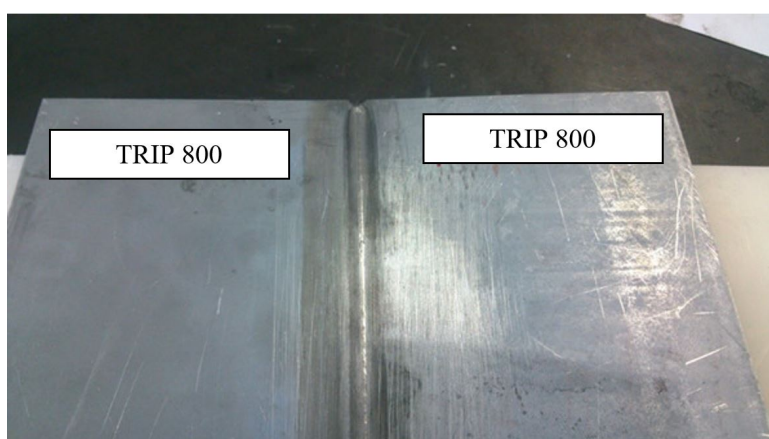

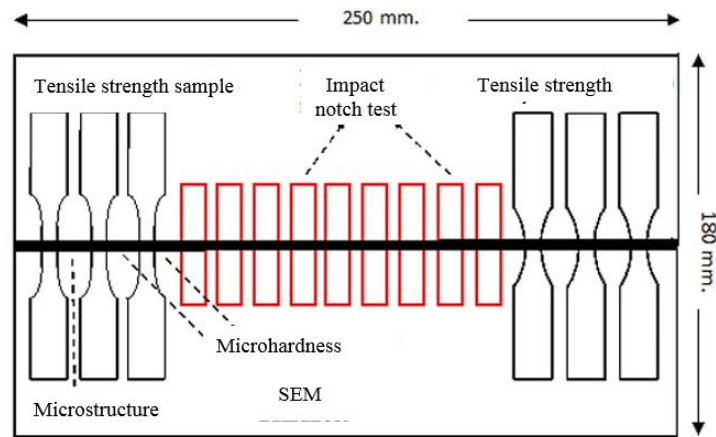**Figure 1.** TRIP 800-TRIP 800 welding sample.
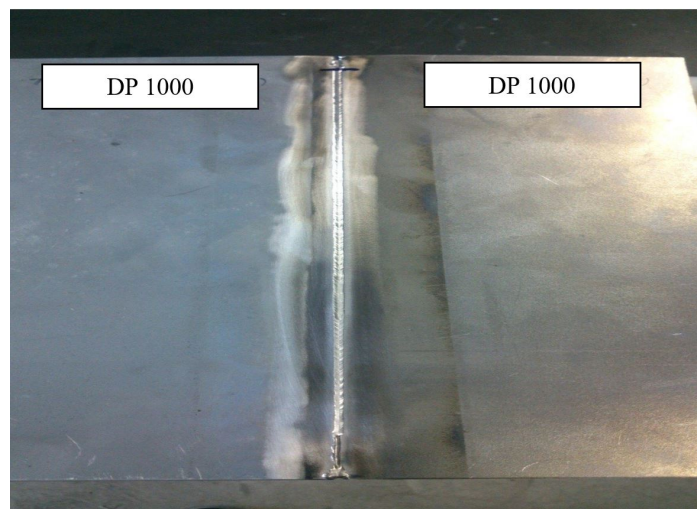
Figure 2. Schema of the samples.

Figure 3. DP 1000-DP 1000 welding sample.

The samples were sanded with mesh water abrasive from 240 to 3000. Then all the samples were polished with 3 μm diamond paste. The etching was carried out with a mixture of nital 2%. The sample was left in this mixture for 12 seconds.

Vickers (HV 0.2) hardness measurements were carried out from the base metal toward FZ with a load of 200 g for 15 seconds.

Impact notch test sample was carried out at -20 °C and room temperature (20 °C). Three samples were used to find the average values of the samples (DP 1000- DP 1000 and TRIP 800-TRIP 800) at both temperatures.

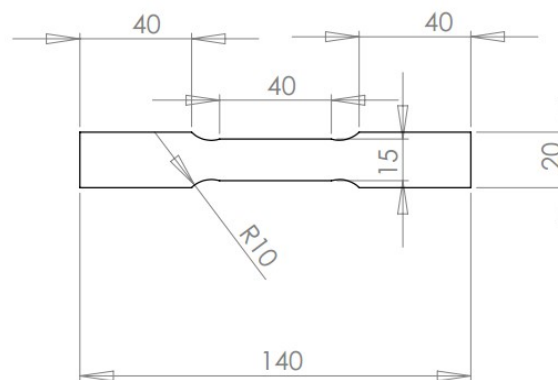The technical drawing of the samples prepared for the tensile test is shown in Figure 4.

Figure 4. Tensile strength sample (Unit of measurement is mm). R: radius.

3. Result and Discussions

3.1. Microstructure

Figure 5 and Figure 6 show that three zones were observed in heat affected zone (HAZ). These were coarse-grained HAZ (CG-HAZ), fine-grained HAZ (FG-HAZ) and tempered HAZ (T-HAZ). The CG-HAZ was observed at near fusion zone, T-HAZ was observed at the near base metal zone and FG-HAZ was observed between CG-HAZ and T-HAZ.

Figure 7a shows the base metal of TRIP 800. The matrix of the microstructure consisted of ferrite. Chiang et al. (2011) reported that, in the SEM micrographs, ferrite seemed dark while martensite and retained austenite (M/RA) seemed light and smooth. Bainite appeared as a nonuniform phase contiguous to the M/RA islands [25]. Bainite also appeared as a long and light shape [26]. Figure 7b shows the base metal of DP 1000. Martensite islands consisted of in the ferrite matrix. It was seen that martensite spread in the ferrite matrix. Figure 8 shows the fusion zone (FZ) of TRIP 800 (Figure 8a). FZ also contained martensite and austenite was seen at the same SEM photo. FZ of DP 1000 consists almost only of martensite (Figure 8b). FZ consisted martensite in as much as temperature was above the melting point. This microstructure in FZ caused higher hardness than the base metal.
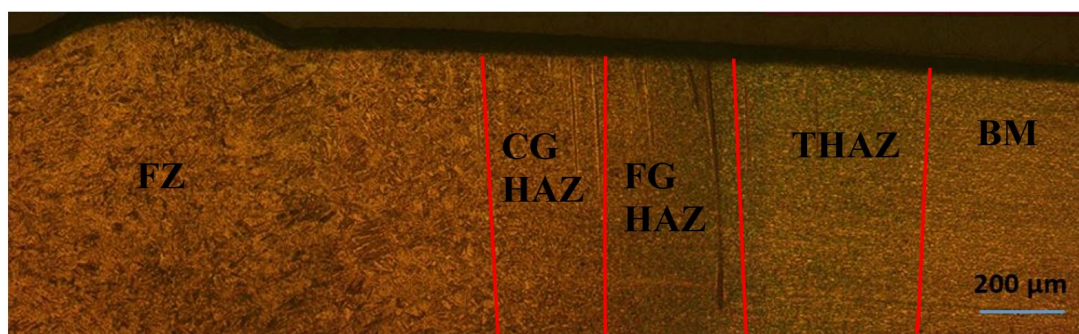

Figure 5. Schematic of cross section of EBW TRIP 800- TRIP 800 joint. FZ: fusion zone; CGHAZ: coarse grain HAZ; FGHAZ: fine grain HAZ; THAZ: tempered zone HAZ; BM: base metal.
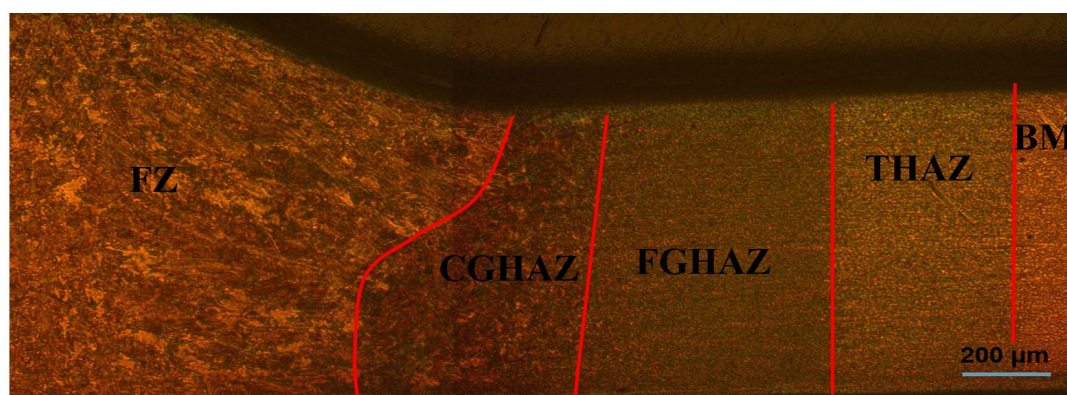

Figure 6. Schematic of cross section of EBW DP 1000- DP 1000 joint. FZ: fusion zone; CGHAZ: coarse grain HAZ; FGHAZ: fine grain HAZ; THAZ: tempered zone HAZ; BM: base metal.
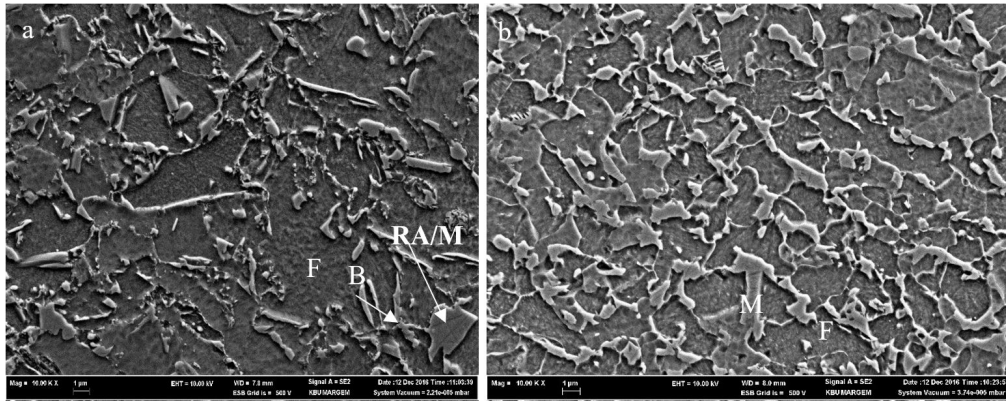
Figure 7. Base metal of (a) TRIP 800; (b) DP 1000. F: ferrite; RA/M: retained austenite/martensite; B: bainite; M: martensite.
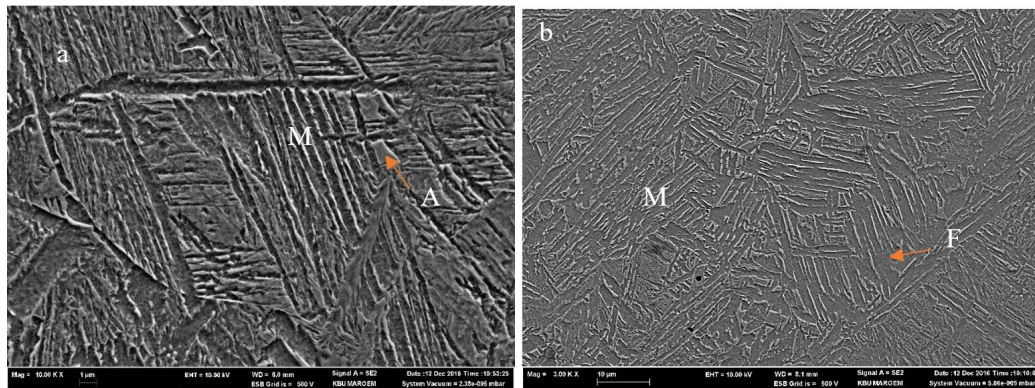
Figure 8. FZ of (a) TRIP 800; (b) DP 1000 (SEM image). **Figure 9 s**hows the HAZ of TRIP 800 (d, e and f) and DP 1000 (a, b and c) joinings. M: martensite, A: austenite, F: ferrite.

The martensite volume of CGHAZ of DP 1000 was more than the THAZ and FGHAZ of DP 1000. Undissolved ferrite was observed at all three figures of DP 1000. The martensite and bainite volume of CGHAZ of TRIP 800 was more than THAZ and FGHAZ of TRIP 800. It was thought that the amount of bainite decreased from FGHAZ to THAZ. Austenite was observed at all three figures of TRIP 800 HAZ.

Figure 9. HAZ of DP 1000 (a) CGHAZ; (b) FGHAZ; (c) THAZ; HAZ of TRIP 800; (d) CGHAZ; (e) FGHAZ; and (f) THAZ. A: austenite; M: martensite; F: ferrite; B: bainite.
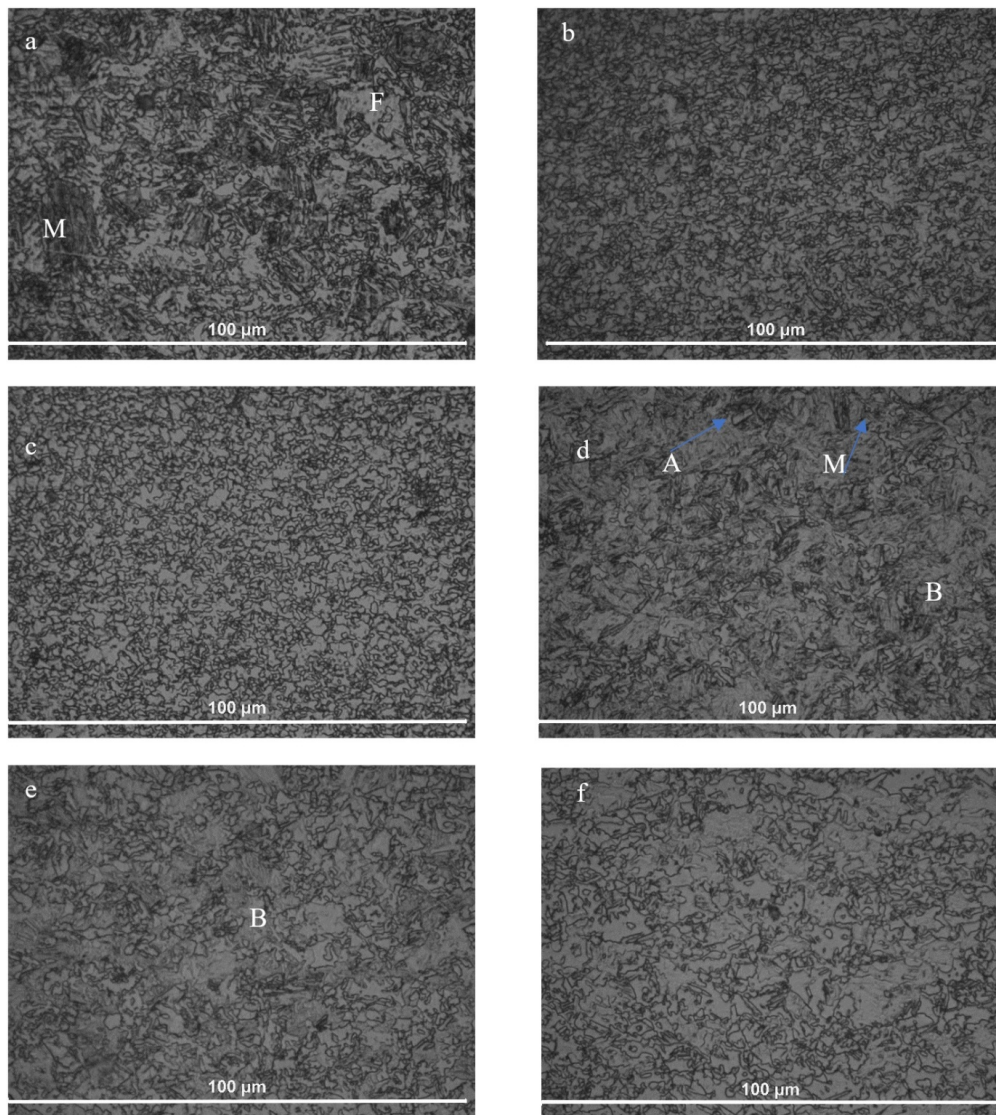
3.2. Microhardness test

The microhardness profile is shown in Figure 10. The average hardness of TRIP 800 FZ, HAZ and base metal was calculated as 442, 301 and 237 HV, respectively. The FZ of TRIP 800 joining exhibited the highest hardness (465 HV) due to hard martensite structure. With the increase in the distance from CGHAZ to the base metal, the volume of martensite decreased (Figure 9d-f). The decrease in the volume of the martensite affected the hardness of HAZ. Grajcar et al. (2014) welded TRIP steel by laser welding. They observed that the highest hardness was in the fine-grained HAZ and it was almost twice higher than the base metal. They mentioned that martensitic-bainitic laths increased its hardness significantly [27]. In the present study, the martensitic laths increased significantly at FZ (Figure 8a). The highest hardness was observed at FZ. Another research in literature mentioned that the overall hardness of the base metal decreased with increasing Ni-content. FZ was observed in the softest zone in their study. High Ni rate decreased both FZ and HAZ [28]. Various researchers reported that slower welding speeds caused homogeneous hardness profile between FZ and base metal at TRIP steel welded by using EBW [19]. However, in the present study, the welding speed was slower than the study mentioned above (the speed in the present study is approximately 3 mm/s slower than theirs) and heterogeneous hardness patterns were observed at the base metal and FZ. The TRIP steel in the study mentioned above contains more chromium and nickel than the TRIP steel used in the present study. The TRIP steel used in this study involved less alloy element, especially Ni, which caused more heterogeneous hardness between FZ and base metal at TRIP steel.

Regarding the average hardness of the DP 1000-DP 1000 joining, FZ, HAZ and base metal were calculated as 307, 256 and 254 HV, respectively. The hard martensitic structure was observed at FZ (Figure 8b). Thus, these structures caused FZ to become the highest hardness zone at DP 1000. Manganese (Mn) and silicon (Si) increased the martensitic formation in FZ and CGHAZ [20]. Figure 9a-c shows

the presence of martensite and ferrite. By moving from the weld fusion zone centerline to the DP 1000 base metal, the volume of ferrite increased but martensite volume decreased.

Wang et al. (2016) carried out laser welding on DP 1000 steel. They observed that the highest hardness values were observed in the fusion zone and reached a maximum of more than 400 HV [29]. Dong et al. (2014) observed that the maximum hardness of FZ of DP 600 steel was 340 HV [30]. Jia et al. (2016) observed that the maximum hardness was in the FZ of DP 600 and DP 980 and it was higher than 400 HV [31]. In the present study, the hardness of the fusion zone of DP was lower than the above-cited studies. The results showed two reasons for the softening. Firstly, when DP 1000 steel reached the intercritical temperature, harder martensite transformed to tempered martensite. Secondly, the precipitation of carbides occurred in this temperature [32]. Furthermore, it can be said that the vacuum cabin at EBW influenced the cooling rate of metal. As the vacuum cabin can cause slower cooling according to laser welding, it can cause low hardness values. Retained austenite transformed into martensite or bainite with increasing temperature. This transformation caused more martensitic and bainitic structure in TRIP 800 according to DP 1000, which in turn caused the hardness of HAZ and FZ of TRIP steel to become higher than the HAZ and FZ of DP 1000. Therefore, it was thought that vacuum cabin affected the hardness of HAZ and FZ of TRIP 800. Nayak et al. (2012) investigated the comparing microstructure and mechanical properties of fusion zones of TRIP steels in resistance spot welding and laser welding. One particular sample in their study was almost the same as chemically and in terms of its mechanical properties with TRIP 800 used in the present study. The average fusion zone hardness of the TRIP steel in RSW and laser welding was observed as 526 and 484 HV, respectively. As RSW had higher rate of cooling than laser welding, RSW lead to higher hardness than laser welding in the fusion zone [33]. In the present study, the average fusion zone hardness of TRIP 800 was found as 442 HV. When the present study is compared with the study of Nayak et al., it can be said that vacuum cabin could affect the hardness of TRIP 800 and the hardness of DP 1000.
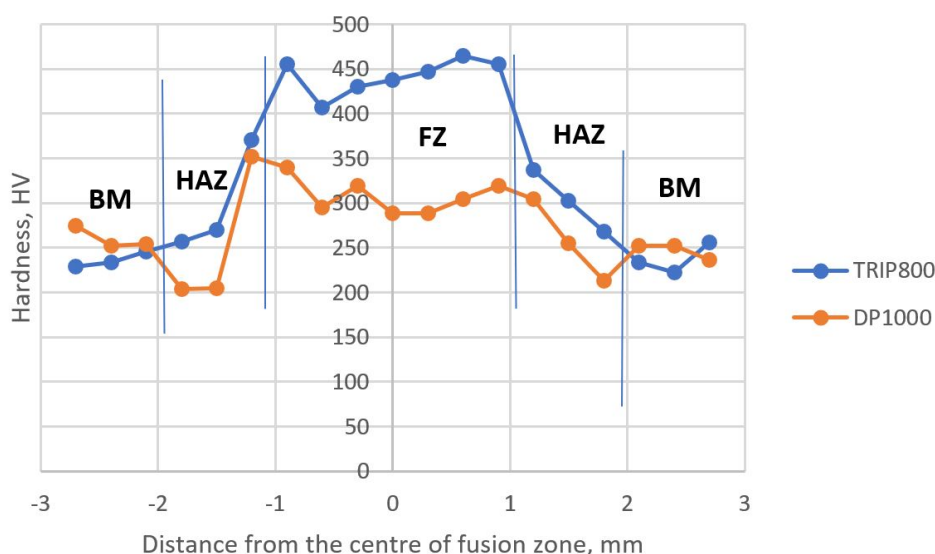

Figure 10. Hardness **graphic of** samples. BM: Base metal; HAZ: heat affected zone; FZ: fusion zone.

3.3. Charpy impact notch test results

The impact notch tests were carried out at 20 °C (room temperature) and -20 °C. The Charpy V-notch in the weld joints was located at the weld centre line for each sample. Some researcher used to calculate fracture energy by using formula [34] but in this study we used Charpy impact notch test machine. For the calculation of the average fracture energy, three samples were used at the same temperature. Figure 11 shows shape of separate Charpy notched test sample. Figure 12 shows the average fracture energy of TRIP 800-TRIP 800 and DP 1000-DP 1000 welded at 20 °C and -20 °C.
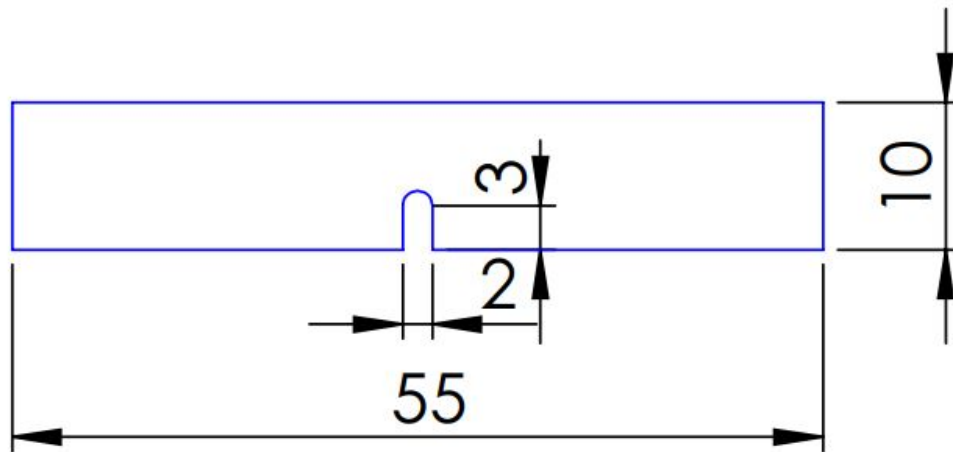
Figure 11. Shape of separate Charpy notched test sample. Unit of measurement is mm.
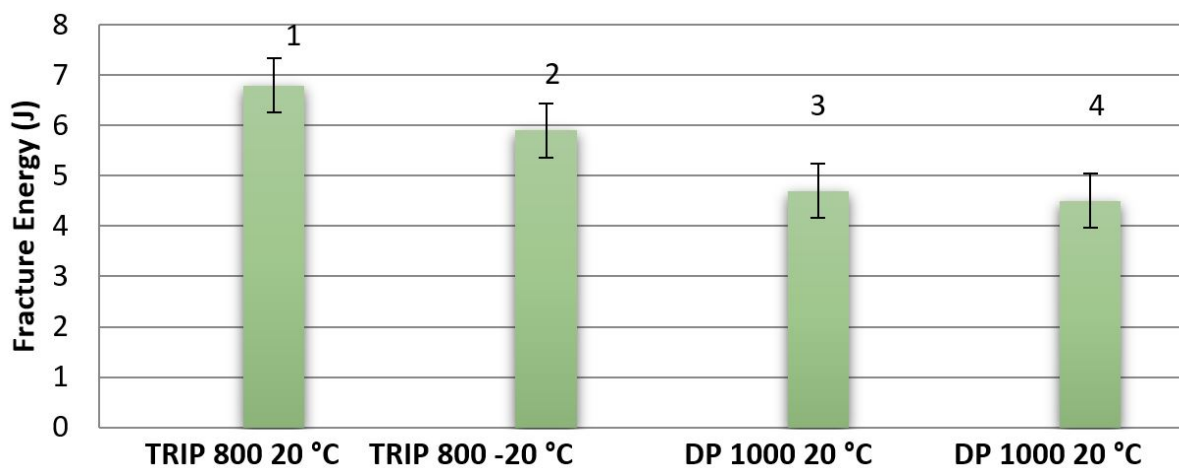

Figure 12. Average of Samples Fracture Energies 1. TRIP 800-TRIP 800 at 20 °C 2. TRIP 800-TRIP 800 at -20 °C, 3.DP 1000-DP 1000 at 20 °C, 4. DP 1000-DP 1000 at -20 °C.

As can be seen in Figure 12, the TRIP 800-TRIP 800 joining had the highest average fracture energy with 6,8 J at room temperature. The average fracture energy of TRIP 800-TRIP 800 at -20 °C was 5.9 J. However, DP 1000-DP 1000 had minimum average fracture energy with 4,5 J at -20 °C and its average fracture energy was 4,7 J at room temperature. Both at room temperature and at -20 °C, the fracture energy of the TRIP 800 joinings was better than the DP 1000 joinings. These results show that the TRIP 800-TRIP 800 EBW samples had better impact toughness values than DP 1000- DP 1000 EBW at both room temperature and -20 °C. The transformation of austenite to martensite in the TRIP steels exhibited various advantages such as energy absorption at dynamic tests [6]. This transformation influenced the fracture energy of TRIP 800 positively.

Figures 13 and 14 show the SEM images of impact test samples. Both samples had a large number of dimples at the fracture surface at room temperature and -20 °C. When two samples (TRIP 800-TRIP 800 and DP1000-DP 1000) were compared, the TRIP 800 joining had more dimples than DP 1000 at both temperatures. No similar study on the impact notch test results of welding TRIP steel or DP steel by using EBW was found in the literature to compare the results of this study.
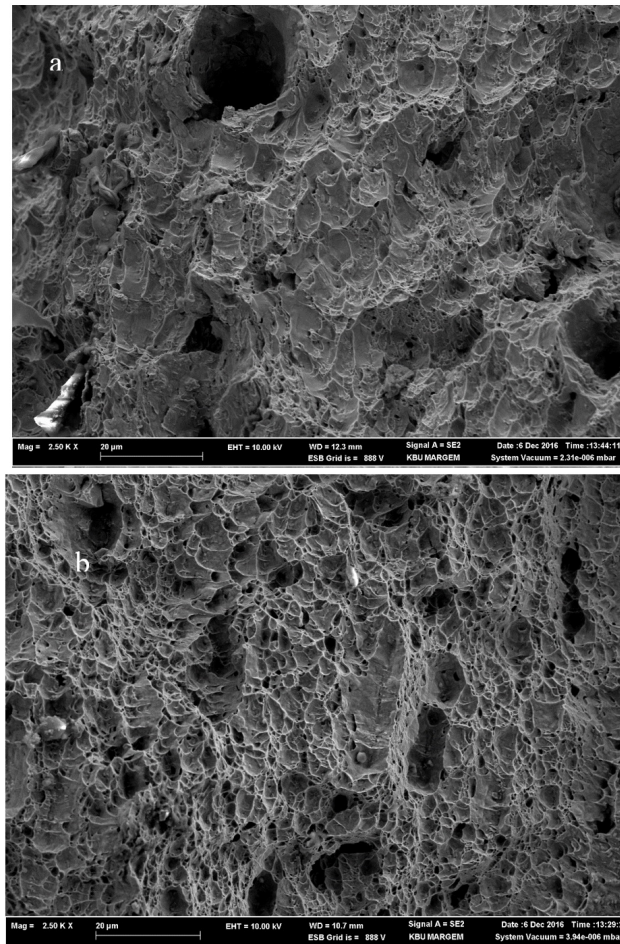
Figure 13. (a) DP 1000-DP 1000 impact test at room temperature; (b) TRIP 800-TRIP 800 impact test at room temperature.
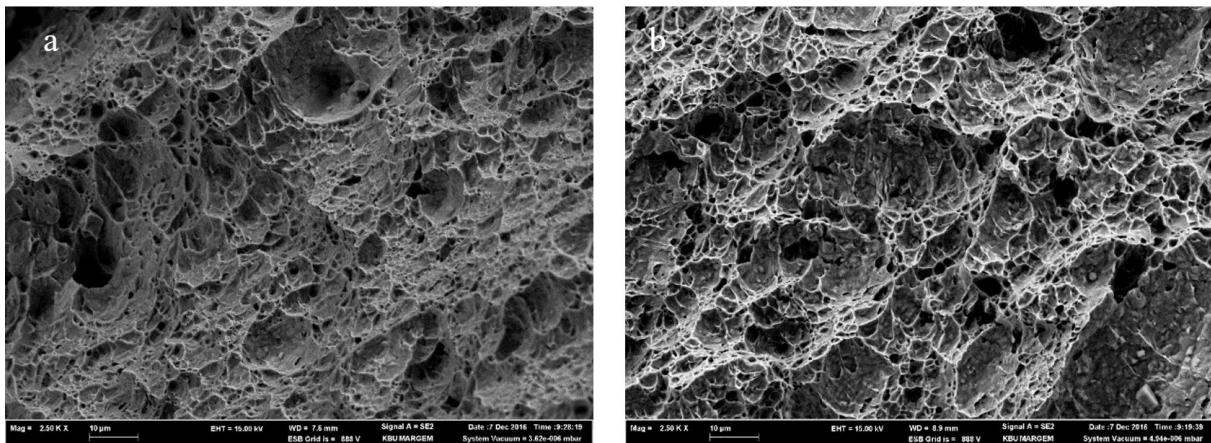

Figure 14. (a) DP 1000-DP 1000 impact test at -20 °C; (b) TRIP 800-TRIP 800 impact test at -20 °C.

3.4. Tensile strength test

The results of the tensile strength tests were showed in Table 4. The speed used for all configurations in the tensile was 2.0 mm/min. Extensometer was used for measure changes in the length of samples. Although the DP 1000-DP 1000 welded joints were broken from HAZ, the TRIP 800 -TRIP 800 welded joints were broken from the base metal. Figure 11 shows that the minimum hardness was observed at the HAZ of the DP 1000 joinings and base metal of TRIP 800. Thus, it can be said that soften zones affected the tensile strength of the joinings. Halbauer et al. (2016) observed no significant influence on the mechanical properties (tensile strength and elongation) of electron beam welded metal compared to the base metal [19]. On the contrary, in this present study, it was seen that the highest tensile strength (averagely 840 MPa) and elongation (averagely 23%) values were observed at the TRIP 800-TRIP 800 welded joint. It can be said that the tensile strength of the welded steel was close to

the value of the base metal at TRIP 800 joining while the elongation value of the welded steel decreased significantly due to the increasing volume of martensite at FZ (Figures 8a and 9a).

Table 4. Tensile test results of welded materials.

Materials	Yield Strength (MPa)	Tensile strength (MPa)	Elongation (%)
TRIP 800-TRIP 800	439±8	840±4	23±0.5
DP 1000-DP 1000	463±3	656±3	4±0.3

The DP 1000-DP 1000 welded joints were broken from HAZ. Its average tensile strength and elongation were 656 MPa and 4%, respectively. The tempering martensite caused softening in the HAZ of the DP980 steels [35,36]. The volume of martensite in base metal affected the size of softening [37]. As EBW was carried out in vacuum atmospheric, the air contact of the samples was delayed and the cooling process became slower. Thus, the martensite phase became softer by tempering while staying at high temperature for a long time. This could affect the microstructure in the HAZ and cause to get low tensile strength value.

The tensile test showed that the TRIP 800 joinings were more ductile than the DP 1000 joinings. It was also seen that the HAZ of TRIP 800 joining included retained austenite (Figure 9d). It could affect TRIP 800 joinings ductility positively.

Figures 14 and 15 show the SEM fractography of the tensile fracture surface. The fracture surface showed no significant differences between TRIP 800 and DP 1000 welded joints. Not only large amounts but also small dimples can be observed at both of the fracture surfaces of steels in Figures 15 and 16.
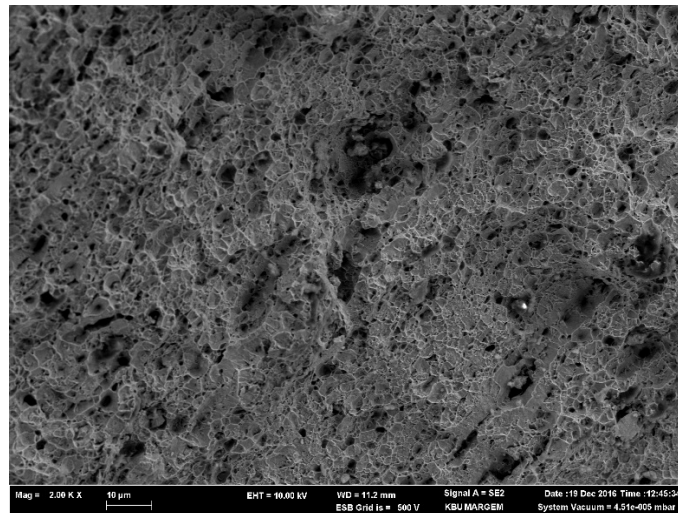

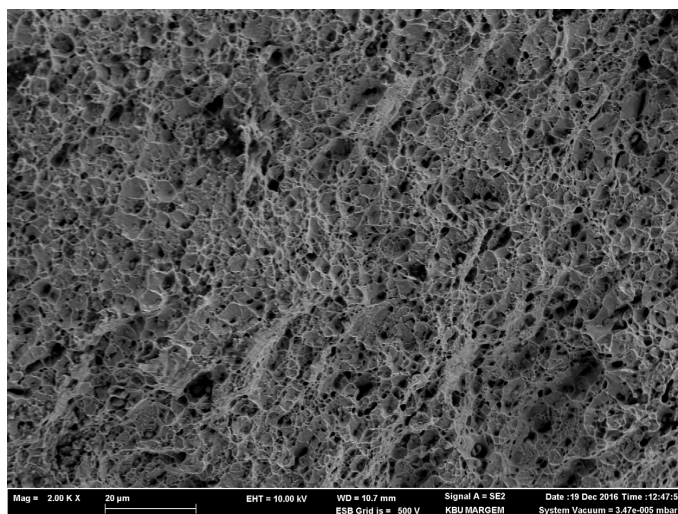**Figure 15.** TRIP 800-TRIP 800 tensile strength SEM image.

Figure 16. DP 1000-DP 1000 tensile strength SEM image.

4. Conclusions

- FZ composed almost only of martensite at both of the joinings (TRIP800-TRIP800, DP1000-DP1000). While the HAZ of the TRIP 800 joining composed of martensite, austenite and bainite, the HAZ of the DP 1000 joining composed of martensite and ferrite. The ferrite volume increased from CGHAZ towards THAZ;

- The hardest point was observed in the FZ of the TRIP 800 joining (465 HV 0.2) and CGHAZ of DP 1000 (352 HV 0.2) due to the occurring martensite phase. However, the highest average hardness was observed at the FZ of both steel joinings due to the presence of the martensite phase. The hardness of the TRIP 800 joining was higher than the DP 1000 joining. It was thought that the retained austenites in TRIP 800 steel could form martensite and bainite after post-weld cooling. Thus, the martensite and bainite volume at FZ of TRIP 800 joining could be more than DP 1000 joining FZ. It was observed that the hardness decreased for each joining as it moved from CGHAZ to THAZ. While the ferrite volume increased at the DP 1000 joining, bainite and martensite volume decreased at the TRIP 800 joining as it moved from CGHAZ to THAZ;

- Impact energy tests show that the TRIP 800 joinings (6,8 J at room temperature and 5.9 J at -20 °C) had higher impact energy than DP 1000 joinings (4,7 J at room temperature and 4,5 J at -20 °C) at each temperature. The transformation of austenite to martensite exhibits beneficial properties at TRIP steels, particularly ductility and energy absorption. This benefit was observed at the tensile strength test;

- DP 1000 joinings broke in HAZ but TRIP 800 joinings broke in the base metal. Softening zone (HAZ of DP 1000 joining) influenced the tensile property of DP 1000 weld joints. While the tensile strength of DP 1000 joinings decreased 40% and elongation decreased 50% according to the DP 1000 base metal. Tensile strength didn't decrease at a high rate (5%) but elongation decreased by more than 30% at TRIP 800 joinings according to the base metal. It was thought that the transformation of austenite to martensite prevented a decrease in tensile strength and elongation as it seems in DP 1000 joinings.

Acknowledgements

References

[1] World Auto Steel Association. Advanced high-strength steels application guidelines version 6.0. Brussels: WorldAutoSteel; 2017.

[2] De Cooman BC. Structure-properties relationship in TRIP steels containing carbide-free bainite. Current Opinion in Solid State and Materials Science. 2004;8(3-4):285-303. http://dx.doi.org/10.1016/j.cossms.2004.10.002.

[3] Hayat F. The investigation of the use of TRIP steels in automotive industry. Journal of the Faculty of Engineering and Architecture of Gazi University. 2010;25(4):701-712. [access 4 mar 2020]. Available from: http://static.dergipark.org.tr/article-download/imported/1061000480/1061000448.pdf

[4] Mertinger V, Nagy E, Tranta F, Solyom J. Strain-induced martensitic transformation in textured austenitic stainless steels. Materials Science and Engineering A. 2008;481-482:718-722. http://dx.doi.org/10.1016/j.msea.2007.02.165.

[5] Galán J, Samek L, Verleysen P, Verbeken K, Houbaert Y. Advanced high strength steels for automotive industry. Revista de Metalurgia. 2012;48(2):118-131. http://dx.doi.org/10.3989/revmetalm.1158.

[6] Oliver S, Jones TB, Fourlaris G. Dual phase versus TRIP strip steels: comparison of dynamic properties for automotive crash performance. Materials Science and Technology. 2013;4:423-431. http://dx.doi.org/10.1179/174328407X168937.

[7] Ramazani A, Mukherjee K, Schwedt A, Goravanchi P, Prahl U, Bleck W. Quantification of the effect of transformation-induced geometrically necessary dislocations on the flow-curve modelling of dual-phase steels. International Journal of Plasticity. 2013;43:128-152. http://dx.doi.org/10.1016/j.ijplas.2012.11.003.

[8] Asadi M, De Cooman BC, Palkowski H. Influence of martensite volume fraction and cooling rate on the properties of thermomechanically processed dual phase steel. Materials Science and Engineering A. 2012;538:42-52. http://dx.doi.org/10.1016/j.msea.2012.01.010.

[9] Speich GR. ASM handbook. Vol. 1. Materials Park: The Materials Information Company; 1993. p. 1102-1118.

[10] Węglowski MS, Błacha S, Phillips A. Electron beam welding – techniques and trends – review. Vacuum. 2016;130:72-92. http://dx.doi.org/10.1016/j.vacuum.2016.05.004.

[11] Guo S, Zhou Q, Kong J, Peng Y, Xiang Y, Luo TY, et al. Effect of beam offset on the characteristics of copper/304stainless steel electron beam welding. Vacuum. 2016;128:205-212. http://dx.doi.org/10.1016/j.vacuum.2016.03.034.

[12] Hajitabar A, Naffakh-Moosavy H. Electron beam welding of difficult-to-weld austenitic stainless steel/Nb-based alloy dissimilar joints without interlayer. Vacuum. 2017;146:170-178. http://dx.doi.org/10.1016/j.vacuum.2017.09.046.

[13] Rocha ICL, Machado IG, Mazzaferro CCP. Mechanical and metallurgical properties of DP 1000 steel square butt welded joints with GMAW. IACSIT International Journal of Engineering and Technology. 2014;4(1):26-34. http://dx.doi.org/10.14419/ijet.v4i1.3928.

[14] Varol F, Ekici M, Ferik E, Ozsarac U, Aslanlar S. Investigation of mechanical properties of MIG-Brazed TRIP 800 steel joints using different working angles. Acta Physica Polonica A. 2015;127(4):965-967. http://dx.doi.org/10.12693/APhysPolA.127.965.

[15] López Cortéz VH, Pérez Medina GY, Reyes Valdéz FA, López HF. Effects of the heat input in the mechanical integrity of the welding joints welded by GMAW and LBW process in Transformation Induced Plasticity steel (TRIP) used in the automotive industry. Soldagem e Inspeção. 2010;15(3):234-241. http://dx.doi.org/10.1590/S0104-92242010000300010.

[16] Di H, Sun Q, Wang X, Li J. Microstructure and properties in dissimilar/similar weld joints between DP780 and DP980 steels processed by fiber laser welding. Journal of Materials Science and Technology. 2017;33(12):1561-1571. http://dx.doi.org/10.1016/j.jmst.2017.09.001.

[17] Sevim I. Newly revealed features of fracture toughness behavior of spot welded dual phase steel sheets for automotive bodies. Materials Testing. 2015;57(11-12):960. http://dx.doi.org/10.3139/120.110798.

[18] Sevim I. An experimental study on fracture toughness of resistance spot welded galvanized and ungalvanized DP 450 steel sheets used in automotive body. Revista de Metalurgia. 2016;52(3):e072. http://dx.doi.org/10.3989/revmetalm.072.

[19] Halbauer L, Eckner R, Wendler M, Fabrichnaya O, Buchwalder A, Krüger L, et al. tensile behavior of cast and electron beam welded interstitially strengthened high-alloy TRIP steel. Steel Research International. 2016;87(12):1627-1637. http://dx.doi.org/10.1002/srin.201600028.

[20] Hayat F. Comparing properties of adhesive bonding, resistance spot welding, and adhesive weld bonding of coated and uncoated DP 600 steel. Journal of Iron and Steel Research International. 2011;18(9):70-78. http://dx.doi.org/10.1016/S1006-706X(12)60037-5.

[21] Halbauer L, Buchwalder A, Zenker R, Biermann H. The influence of dilution on dissimilar weld joints with high-alloy TRIP/TWIP steels. Welding in the World. 2016;60(4):645-652. http://dx.doi.org/10.1007/s40194-016-0324-x.

[22] Borrmann S, Kratzsch C, Halbauer L, Buchwalder A, Biermann H, Saenko I, et al. Electron beam welding of CrMnNi-steels: CFD-modeling with temperature sensitive thermophysical properties. International Journal of Heat and Mass Transfer. 2019;139:442-455. http://dx.doi.org/10.1016/j.ijheatmasstransfer.2019.04.125.

[23] Kasonde M. Optimizing the mechanical properties and microstructure of armoured steel plate in quenched and tempered condition [thesis]. South Africa: University of Pretoria; 2006.

[24] Langdon GS, Nurick GN, Balden VH, Timmis RB. Perforated plates as passive mitigation systems. Defence Science Journal. 2008;58(2):238-247. http://dx.doi.org/10.14429/dsj.58.1644.

[25] Chiang J, Lawrence B, Boyd JD, Pilkey AK. Effect of microstructure on retained austenite stability and work hardening of TRIP steels. Materials Science and Engineering A. 2011;528(13-14):4516-4521. http://dx.doi.org/10.1016/j.msea.2011.02.032.

[26] Pereloma E, Edmonds DV. Phase transformations in steels. Vol. 2. Oxford: Elsevier; 2012. 229 p.

[27] Grajcar A, Rozanski M, Stano S, Kowalski A. Microstructure characterization of laser-welded Nb-microalloyed silicon-aluminum TRIP steel. Journal of Materials Engineering and Performance. 2014;23(9):3400-3406. http://dx.doi.org/10.1007/s11665-014-1118-1.

[28] Halbauer L, Zenker R, Weidner A, Buchwalder A, Biermann H. Electron beam welding of cold rolled high-alloy TRIP/TWIP steel sheets. Steel Research International. 2016;87(4):436-444. http://dx.doi.org/10.1002/srin.201500086.

[29] Wang J, Yang L, Sun M, Liu T, Li H. Effect of energy input on the microstructure and properties of butt joints in DP1000 steel laser welding. Materials & Design. 2016;90:642-649. http://dx.doi.org/10.1016/j.matdes.2015.11.006.

[30] Dong D, Liu Y, Yang Y, Li J, Ma M, Jiang T. Microstructure and dynamic tensile behavior of DP600 dual phase steel joint by laser welding. Materials Science and Engineering A. 2014;594:17-25. http://dx.doi.org/10.1016/j.msea.2013.11.047.

[31] Jia Q, Guo W, Li W, Zhu Y, Peng P, Zou G. Microstructure and tensile behavior of fiber laser-welded blanks of DP600 and DP980 steels. Journal of Materials Processing Technology. 2016;236:73-83. http://dx.doi.org/10.1016/j.jmatprotec.2016.05.011.

[32] Wang J, Yang L, Sun M, Liu T, Li H. A study of the softening mechanisms of laser-welded DP1000 steel butt joints. Materials & Design. 2016;97:118-125. http://dx.doi.org/10.1016/j.matdes.2016.02.071.

[33] Nayak SS, Baltazar Hernandez VH, Okita Y, Zhou Y. Microstructure–hardness relationship in the fusion zone of TRIP steel welds. Materials Science and Engineering A. 2012;551:73-81. http://dx.doi.org/10.1016/j.msea.2012.04.096.

[34] Sevim I. Fracture toughness of spot-welded steel joints. Kovove Materialy. 2005;43:113-123. [access 4 mar 2020]. Available from: http://www.kovmat.sav.sk/abstract.php?rr=43&cc=2&ss=113

[35] Bandyopadhyay K, Panda SK, Saha P. Optimization of fiber laser welding of DP980 steels using RSM to improve weld properties for formability. Journal of Materials Engineering and Performance. 2016;25(6):2462-2477. http://dx.doi.org/10.1007/s11665-016-2071-y.

[36] Bandyopadhyay K, Panda SK, Saha P, Baltazar-Hernandez VH, Zhou YN. Microstructures and failure analyses of DP980 laser welded blanks in formability context. Materials Science and Engineering A. 2016;652:250-263. http://dx.doi.org/10.1016/j.msea.2015.11.091.

[37] Zhao YY, Zhang YS, Hu W. Effect of welding speed on microstructure, hardness and tensile properties in laser welding of advanced high strength steel. Science and Technology of Welding and Joining. 2013;18(7):581-590. http://dx.doi.org/10.1179/1362171813Y.0000000140.